Far-field particle manipulation scheme based on X wave

Menyang Gong (宫门阳), **Yupei Qiao** (乔玉配), **Jun Lan** (蓝君), **and Xiaozhou Liu** (刘晓宙)

View Online   Export Citation   CrossMark
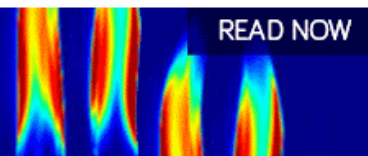
Far-field particle manipulation scheme based on X wave

View Online   Export Citation   CrossMark

Menyang Gong (宫门阳),   **Yupei Qiao (乔玉配),**   **Jun Lan (蓝君), and Xiaozhou Liu (刘晓宙)**[a]

AFFILIATIONS

Key Laboratory of Modern Acoustics, Collaborative Innovation Center of Advanced Microstructures, Institute of Acoustics and School of Physics, Nanjing University, Nanjing 210093, China

[a]Author to whom correspondence should be addressed: xzliu@nju.edu.cn. **Also at:** State Key Laboratory of Acoustics, Institute of Acoustics, Chinese Academy of Sciences, Beijing 100190, China.

ABSTRACT

The construction of particle manipulation in the near-field sound field has been extensively studied. In this article, a scheme for far-field particle control through a non-diffracted wave based on the X wave is proposed, which has theoretical completeness and algorithmic simplicity for the construction of far-field acoustic tweezers. The analytical expression of the acoustic radiation force (ARF) acting upon spherical particles of any order X wave is deduced. The spectral pattern of ARF exerted by the X wave in the fluid medium is given. The change law of ARF exerted by the X wave with specific parameters is obtained through calculation. Through the drawn image, the possibility of obtaining a wide range of negative ARFs through X wave is verified. In addition, the far-field invariance of the ARF exerted by the X wave as non-diffraction wave is verified, which provides the possibility of the subsequent construction of far-field acoustic tweezers as well as the basis algorithms for designing acoustic schemes for specific particle manipulation.

Published under license by AIP Publishing. https://doi.org/10.1063/5.0027525

I. INTRODUCTION

Previously, Ashkin achieved the capture and control of microscopic particles by constructing optical tweezers.[1] However, due to the limitations of electromagnetic waves, there are several disadvantages: Optical tweezers can only be applied to transparent media. A high local energy produces more obvious thermal effects. The size of the manipulated particles is generally from the elementary particle to the atomic scale. In order to circumvent these shortcomings, the "acoustical tweezers" were proposed by Wu in 1991.[2] Acoustic tweezers constructed with sound waves perform better in the face of the above questions, and the scale of the manipulated particles has been extended to the order of cells to tissues. Therefore, the construction of acoustic tweezers has a very broad application prospect in fields such as medical manipulation. In recent research in the field of fluids, the manipulation of particles is an important hot topic.[3–8] "Acoustic tweezers" are an effective and important conception of particle manipulation in fluids. Acoustic tweezers mainly rely on the acoustic radiation force (ARF) of sound waves to establish potential wells. It is of great significance to study the ARF exerted by various types of sound waves upon various particles in various media to achieve particle manipulation.[9–16] The ARF exerted by the plane wave, Gaussian wave, and Bessel wave on spherical particles and cylindrical particles has been widely studied.[9,17–39] General acoustic waves have the property of far-field diffusion due to diffraction, which causes great difficulties in the process of manipulating far-field particles. Therefore, studying the ARF exerted by sound waves with far-field construction ability is of great significance to the far-field realization of acoustic tweezers. As an important type of the non-diffraction wave, the X wave has been widely used in high-resolution imaging, remote sensing, material characterization, and other fields.[40,41] Due to its non-diffraction nature, the sound radiation force in the far field has a strong instrumental value.

II. THE SUPERIORITY, COMPLETENESS, AND ALGORITHM SIMPLICITY OF X WAVE FOR FAR-FIELD SOUND FIELD ENVIRONMENT DESIGN

For a non-diffraction wave, the sound pressure needs to satisfy the wave equation,

$$\frac{1}{\rho}\frac{\partial}{\partial \rho}\left(\rho\frac{\partial p}{\partial \rho}\right) + \frac{1}{\rho^2}\frac{\partial^2 p}{\partial \phi^2} + \frac{\partial^2 p}{\partial z^2} = \frac{1}{c_0^2}\frac{\partial^2 p}{\partial t^2}, \tag{1}$$

and non-diffraction conditions,

$$p(\rho, \phi, z, t) = p(\rho, \phi, z + \Delta z_0, t + \Delta t_0), \tag{2}$$

$$\Delta t_0 = \frac{\Delta z_0}{V}. \tag{3}$$

Here, ρ, ϕ, and z represent the radial, angular, and axial parameter of the cylindrical coordinate, respectively. p, c_0, and V stand for the sound pressure, velocity of sound, and the propagation velocity of the wave packet, respectively. It is worth noting that non-diffraction conditions are added to the X wave export process, which intuitively reflect the far-field invariance of sound field construction, from the beginning. For the ARFs used in the acoustic tweezers that involve the nonlinear effect of the sound wave, it is more sensitive to the accuracy control of sound field parameters. In the past, the design of acoustic tweezers was mostly limited to the near field. The introduction of non-diffraction conditions circumvents this difficulty. Without considering viscosity, the design of far-field acoustic tweezers is greatly simplified.

The Fourier transform allows us to isolate the non-diffraction constraints of the sound pressure expression,

$$p(\rho, \phi, z, t) = \sum_{m=-\infty}^{\infty}\int_0^\infty k_\rho dk_\rho \int_0^\infty dk_z$$
$$\times \int_{-\infty}^{\infty} d\omega A_m(k_\rho, k_z, \omega)J_m(k_\rho \rho)e^{i(k_z z + m\phi - \omega t)}. \tag{4}$$

Here, k_ρ, k_z, A_m, and J_m are referred to as the radial wave number in the cylindrical coordinate, the z-axis wave number in the cylindrical coordinate, the m-th amplitude function, and the m-th Bessel function, respectively. Hence, the intuitive constraint is obtained,

$$\omega = Vk_z + 2n\pi\frac{V}{\Delta z_0}. \tag{5}$$

Due to the limitation of the wave equation, the freedom of equation is reduced,

$$k_\rho^2 + k_z^2 = k^2 = \frac{\omega^2}{c_0^2}. \tag{6}$$

We set

$$A_m(k_\rho, k_z, \omega) = B_m(k_z, \omega)\delta\left(k_\rho^2 - \frac{\omega^2}{c_0^2} + k_z^2\right)$$
$$= B_m(k_z, \omega)\frac{1}{2k_\rho}\left[\delta\left(k_\rho + \sqrt{\frac{\omega^2}{c_0^2} - k_z^2}\right)\right.$$
$$\left.+ \delta\left(k_\rho - \sqrt{\frac{\omega^2}{c_0^2} - k_z^2}\right)\right]. \tag{7}$$

Substituting Eqs. (5)–(7) back to Eq. (4), the sound pressure expression of the zeroth order X wave could be greatly simplified,

$$p(\rho, \phi, z, t) = \sum_{m=-\infty}^{\infty}\int_{-\frac{\omega}{c_0}}^{-\frac{\omega}{c_0}} dk_z \int_{-\infty}^{\infty} d\omega$$
$$\times B_m(k_z, \omega)J_m\left(\rho\sqrt{\frac{\omega^2}{c_0^2} - k_z^2}\right)e^{i(k_z z + m\phi - \omega t)}. \tag{8}$$

Since the expression also needs to satisfy the non-diffraction condition [Eq. (2)], we set

$$B_m(k_z, \omega) = \sum_{n=-\infty}^{\infty} C_{n,m}(\omega)\delta\left[\omega - \left(Vk_z + 2n\pi\frac{V}{\Delta z_0}\right)\right]. \tag{9}$$

Here, $C_{n,m}$ is an arbitrary spectrum function. Based on this, the general expression of the non-diffracted acoustic beam can be obtained,

$$p(\rho, \phi, z, t) = \sum_{m=-\infty}^{\infty}\sum_{n=-\infty}^{\infty} p_{m,n}(\rho, \phi, z, t)$$
$$= \sum_{m=-\infty}^{\infty}\sum_{n=-\infty}^{\infty}\frac{1}{V}e^{-i\left(\frac{2n\pi}{\Delta z_0}z - m\phi\right)}$$
$$\times \int_{-\infty}^{\infty} d\omega e^{i\frac{\omega}{V}(z - Vt)}C_{n,m}(\omega)$$
$$\times J_m\left[\rho\sqrt{\left(\frac{1}{c_0^2} - \frac{1}{V^2}\right)\omega^2 + \frac{4n\pi}{V\Delta z_0}\omega - \left(\frac{2n\pi}{\Delta z_0}\right)^2}\right]. \tag{10}$$

In order to compute the integral in Eq. (10), k_z and ω are converted into two variables with high symmetry by substitution,

$$G(\omega, k_z) = \frac{1}{2V}(\omega + Vk_z), \tag{11}$$

$$H(\omega, k_z) = \frac{1}{2V}(\omega - Vk_z). \tag{12}$$

The sound pressure expression can be rewritten as

$$p = \int_{-\infty}^{\infty} dG \int_{-\infty}^{\infty} dH B(G, H)$$
$$\times J_0\left[\rho\sqrt{\left(\frac{V^2}{c_0^2} - 1\right)(G^2 + H^2) + 2\left(\frac{V^2}{c_0^2} + 1\right)GH}\right]$$
$$\times e^{iG(z - Vt)}e^{iH(z + Vt)}. \tag{13}$$

Because of the constraints [Eq. (5)], an impulse function that further reduces the integral order is introduced,

$$B(G, H) = B_g(G) * \delta\left(H - \frac{n\pi}{\Delta z_0}\right). \tag{14}$$

Hence, the integral expression can be easily simplified,

$$p(\rho, z, t) = \frac{\lambda V}{\sqrt{[\lambda V - i(z - Vt)]^2 + \rho^2\left(\frac{V^2}{c_0^2} - 1\right)}}. \tag{15}$$

λ is an arbitrary parameter introduced into the derivation. Since the wave equation is a homogeneous equation, the sound pressure expression obtained by the arrangement also satisfies the wave equation and the non-diffraction condition for the higher order

derivative of the propagation vector [the expression of the propagation vector mentioned is $\lambda V - i(z - Vt)$] from which the sound pressure expression of the q-th-order X wave is derived,

$$p_q(\rho, z, t) = (-1)^q \frac{\partial^q}{\partial[\lambda V - i(z - Vt)]^q}$$
$$\times \frac{\lambda V}{\sqrt{[\lambda V - i(z - Vt)]^2 + \rho^2\left(\frac{V^2}{c_0^2} - 1\right)}}. \quad (16)$$

Due to the arbitrariness of the parameter selection of $B_g(G)$ during the derivation of non-diffraction waves, when $B_g(G)$ is selected as $B_g(G) = J_0(2\sqrt{\lambda_1 G})e^{-\lambda_2 VG}$, the sound pressure is expressed as

$$p(\rho, z, t) = \int_{-\infty}^{\infty} dG J_0\left(2\sqrt{\lambda_1 G}\right)e^{-\lambda_2 VG}$$
$$\times J_0\left[\rho G \sqrt{\frac{V^2}{c_0^2} - 1}\right] e^{iG(z - Vt)}. \quad (17)$$

The sound pressure expression can be organized as

$$p(\rho, z, t) = \frac{1}{\sqrt{[\lambda V - i(z - Vt)]^2 + \rho^2\left(\frac{V^2}{c_0^2} - 1\right)}}$$
$$\times J_0\left[\frac{\rho \lambda_1 \sqrt{\frac{V^2}{c_0^2} - 1}}{[\lambda V - i(z - Vt)]^2 + \rho^2\left(\frac{V^2}{c_0^2} - 1\right)}\right]$$
$$\times e^{\frac{\lambda_1[\lambda V - i(z - Vt)]}{[\lambda V - i(z - Vt)]^2 + \rho^2\left(\frac{V^2}{c_0^2} - 1\right)}}. \quad (18)$$

Since the acoustic wave equation is a homogeneous equation, its integral to an arbitrary constant still satisfies the wave equation, and Eq. (18) can therefore be written as

$$p = \int_{-\infty}^{\infty} d\lambda_1 J_0(2\sqrt{\lambda_3 \lambda_1}) p(\rho, z, t)$$
$$= J_0\left(\sqrt{\frac{V^2}{c_0^2} - 1}\lambda_3 \rho\right) e^{\lambda_3 V + i\lambda_3(z - Vt)}. \quad (19)$$

Equation (19) reveals that the Bessel beam could be constructed by the X wave. Obviously, the X wave can be used for the cylindrical wave expansion as a kind of beam. Therefore, the Bessel wave and X wave can be expressed by each other. It is known that the spatial sound field can be expanded by Bessel waves, so the spatial sound field can also be expanded using a linear combination of the X wave of various orders. In this way, the completeness of constructing a spatial sound field by X waves of each order as the fundamental wave is proved.

In addition, it could be seen that the X wave expressed in elementary function expressions circumvents the iterative process. Using the X wave as the base beam makes the beam analysis process very concise. Obviously, for the general cylindrical expansion that actually uses the Bessel beam as the fundamental wave, the complexity of the algorithm when designing the far-field acoustic tweezers will be significantly higher than the one that can be described by a basic elementary expression X wave

beam. Therefore, the X wave has a significant advantage in algorithm complexity in the subsequent construction of far-field acoustic tweezers.

III. THEORETICAL CALCULATION OF ARF EXERTED BY X WAVE

To determine the acoustic X wave (AXW) Fourier representation, the X wave should satisfy the following wave equation:

$$\nabla^2 \Phi = \frac{1}{c_0^2} \frac{\partial^2 \Phi}{\partial t^2}. \quad (20)$$

The incident wave expression of the X wave is represented as

$$\Phi_{AXW}^i(\boldsymbol{z}, t) = \int_{z^3} d^3 \boldsymbol{k} \int_0^{\infty} dk e^{-i\boldsymbol{k}\boldsymbol{z}} e^{i\omega t} \psi(\boldsymbol{k}, \omega)\delta(\omega - |\boldsymbol{k}|c). \quad (21)$$

Here, ψ has the following expression:

$$\psi(\boldsymbol{k}, \omega) = ie^{-ka} \frac{2\pi}{c\rho_0 \sin\xi} k^{q-2} \delta(\theta_k - \xi). \quad (22)$$

The angle ξ represents the axicon angle. θ_k is the scattering angle. Note that the impulse function here is essentially used to limit the velocity propagating along the z-axis by the wave vector angle. Here, parameter a is introduced to determine the beam width of the X wave. Expanding the components, we get

$$\Psi_{AXW}^i(\boldsymbol{z}, t) = \int_0^{\infty} dk \int_0^{\pi} d\theta_k \int_0^{2\pi} d\theta_k k^2 \sin\theta_k$$
$$\times \frac{i2\pi}{c\rho_0 \sin\xi} k^{q-2} \delta(\theta_k - \xi) e^{-ka} e^{-i\boldsymbol{k}\boldsymbol{z}} e^{ikct}. \quad (23)$$

Integrating the two angle variables, we get

$$\Psi_{AXW}^i(\boldsymbol{z}, t) = \frac{i4\pi^2}{c\rho_0} \int_0^{\infty} dk k^q e^{-ka} e^{-i\boldsymbol{k}\boldsymbol{z}} e^{ikct}. \quad (24)$$

Based on the inverse Fourier transform,

$$f(t) = \mathscr{F}^{-1}(F(\omega)) = \frac{1}{2\pi} \int_{\infty}^{-\infty} F(\omega)e^{i\omega t} d\omega. \quad (25)$$

Here, the $\mathscr{F}^{-1}$ stands for the inverse Fourier transform. Hence, the velocity potential of the incident sound wave can be expressed in the frequency domain as

$$\Psi_{AXW}^i(\boldsymbol{k}, z) = \frac{i2\pi}{c\rho_0} k^q e^{-ka} e^{-i\boldsymbol{k}z}. \quad (26)$$
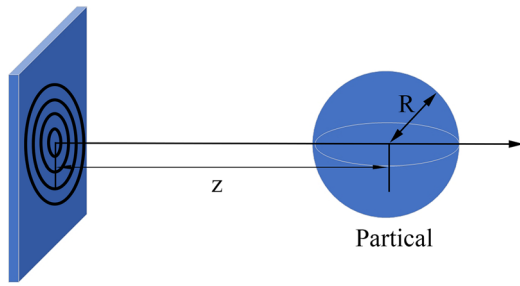
As shown in Fig. 1, Eq. (26) can be expressed as

$$\Psi_{AXW}^i(k, \theta, z) = \frac{i2\pi}{c\rho_0} k^q e^{-ka} e^{-ikz\cos\theta_1}. \quad (27)$$

When the coordinate is transformed into the spherical coordinate centered on the scattering sphere. For the geometric approximation of $z = d \gg R$ in the far field, the relationship is obtained,

$$\sin\theta_1 = \frac{R\sin\theta}{d}. \quad (28)$$

Substituting Eq. (28) into Eq. (27), the simplified expression is obtained,

$$\Psi_{AXW}^i(k, \theta, z) = \frac{i2\pi}{c\rho_0} k^q e^{-ka} e^{-ikz\sqrt{1 - \frac{R^2 \sin^2\theta}{d^2}}}. \quad (29)$$

FIG. 1. Schematic diagram of the X wave acting on a spherical particle.

Similarly, the frequency domain expression of the scattered sound pressure is obtained,

$$
\Psi^s_{AXW}(k, \theta, z) = \frac{i4\pi^2}{c\rho_0} k^q e^{-ka} \sum_{n=0}^{\infty} (-1)^{n+2} (2n+1)
$$
$$
\times \frac{j'(kR) + i\alpha_n j_n(kR)}{h_n^{(2)'}(kR) + i\alpha_n h_n^{(2)}(kR)} h_n^{(2)}(kR)
$$
$$
\times P_n(\cos\theta) P_n(\cos\xi). \tag{30}
$$

The potential in the frequency domain is

$$
\Phi = \Psi_{AXW}(k, \theta, z) = \Psi^i_{AXW}(k, \theta, z) + \Psi^s_{AXW}(k, \theta, z), \tag{31}
$$

$$
\Psi_{AXW}(k, \theta, z) = \frac{i2\pi}{c\rho_0} k^q e^{-ka} \Bigg[e^{-ikz\cos\theta_1} + 2\pi \sum_{n=0}^{\infty} (-1)^{n+2} (2n+1)
$$
$$
\times \frac{j'(kR) + i\alpha_n j_n(kR)}{h_n^{(2)'}(kR) + i\alpha_n h_n^{(2)}(kR)} h_n^{(kz)}
$$
$$
\times P_n(\cos\theta) P_n(\cos\xi) \Bigg]. \tag{32}
$$

Based on the definition of force, the acoustic radiation pressure definition has the expression

$$
\boldsymbol{F} = \iint_{s(t)} (p - p_0)\boldsymbol{n}\,ds - \iint_{s(t)} \rho_0 \left(\frac{\partial \Phi}{\partial t}\right)\boldsymbol{n}\,ds
$$
$$
+ \iint_{s(t)} \frac{1}{2}\rho_0 \left(\frac{\partial \Phi}{\partial z}\right)^2 \boldsymbol{n}\,ds - \iint_{s(t)} \frac{1}{2}\frac{\rho_0}{c^2} \left(\frac{\partial \Phi}{\partial t}\right)^2 \boldsymbol{n}\,ds. \tag{33}
$$

Since $\Phi = \Phi(k, \theta, z)$ is already expressed in the frequency domain, there is an exchangeability of integration due to the continuous function Fourier expansion, i.e.,

$$
\frac{\partial \Phi}{\partial t} = ikc\Phi. \tag{34}
$$

Then, we obtain

$$
\Phi_t = \frac{\partial \Phi}{\partial t} = -\frac{2\pi}{\rho_0} k^{q+1} e^{-ka} \Bigg[e^{-ikz\cos\theta_1} + 2\pi \sum_{n=0}^{\infty} (-1)^{n+2} (2n+1)
$$
$$
\times \frac{j'(kR) + i\alpha_n j_n(kR)}{h_n^{(2)'}(kR) + i\alpha_n h_n^{(2)}(kR)} h_n^{(2)}(kz) P_n(\cos\theta) P_n(\cos\xi) \Bigg], \tag{35}
$$

$$
\Phi_z = \frac{\partial \Phi}{\partial z} = \frac{i2\pi}{c\rho_0} k^q e^{-ka} \Bigg[-ik\cos\theta_1 e^{-ikz\cos\theta_1}
$$
$$
+ 2\pi \sum_{n=0}^{\infty} (-1)^{n+2} (2n+1) \frac{j'(kR) + i\alpha_n j_n(kR)}{h_n^{(2)'}(kR) + i\alpha_n h_n^{(2)}(kR)} h_n^{(2)'}(kz) P_n
$$
$$
\times (\cos\theta) P_n(\cos\xi) \Bigg]. \tag{36}
$$

The integration area is the entire surface of the particle,

$$
\iint_s F(s)\,ds = \int_\phi F_1(\phi)\,d\phi \int_\theta F_2(\theta)\,d\theta\big|_{r=R}. \tag{37}
$$

Due to symmetry, the velocity potential is not a function of the angle ϕ,

$$
\int_\phi d\phi = 2\pi. \tag{38}
$$

Substituting Eqs. (37) and (38) into Eq. (33), the ARF can be obtained as

$$
F = -\iint_\theta 2\pi\rho_0 \left(\frac{\partial \Phi}{\partial t}\right)d\theta + \iint_\theta \pi\rho_0 \left(\frac{\partial \Phi}{\partial z}\right)^2 d\theta
$$
$$
- \iint_\theta \frac{\pi\rho_0}{c^2} \left(\frac{\partial \Phi}{\partial t}\right)^2 d\theta
$$
$$
= -\pi\rho_0 \Bigg[2\int_\theta \left(\frac{\partial \Phi}{\partial t}\right)d\theta - \int_\theta \left(\frac{\partial \Phi}{\partial z}\right)^2 d\theta + \iint_\theta \frac{1}{c^2}\left(\frac{\partial \Phi}{\partial t}\right)^2 d\theta \Bigg]. \tag{39}
$$

We set

$$
A_n = (-1)^{n+2}(2n+1) \frac{j'(kR) + i\alpha_n j_n(kR)}{h_n^{(2)'}(kR) + i\alpha_n h_n^{(2)}(kR)}
$$
$$
\times P_n(\cos\theta) P_n(\cos\xi). \tag{40}
$$

Then, we gain

$$
\Phi_t = -\frac{2\pi}{\rho_0} k^{q+1} e^{-ka} \Bigg[e^{-ikz\cos\theta_1} + 2\pi \sum_{n=0}^{\infty} h_n^{(2)}(kz) * A_n \Bigg], \tag{41}
$$

$$
\Phi_z = \frac{i2\pi}{c\rho_0} k^q e^{-ka} \Bigg[-ik\cos\theta_1 e^{-ikz\cos\theta_1} + 2\pi \sum_{n=0}^{\infty} k * h_n^{(2)'}(kz) * A_n \Bigg]. \tag{42}
$$

Hence, the expression of ARF exerted by the X wave is obtained. In the following, our derivation results are checked by a numerical simulation.

IV. THE RELATIONSHIP BETWEEN THE ARF EXERTED BY THE X WAVE ON SPHERICAL PARTICLES AND VARIOUS PARAMETERS

To verify the theoretical solutions and provide a basis for the next algorithm design, numerical simulations in this section are performed. The numerical simulation is based on the previous theoretical expression. In the theoretical part, it can be deduced that the expression of ARF exerted by the X wave is a multi-parameter expression related to the X wave's order number, the wave number, the angle parameter, the particle radius, and the distance between the target particle and the transducer. In order to explore the change law of ARF exerted by the X wave under a specific parameter, while other non-research parameters are fixed, the numerical simulation is carried out. A unified normalization process is carried out to visualize the law. The normalization method is to make it dimensionless

TABLE I. Related parameters of *Mn*.

Material	*Mn*
Bulk modulus B (10^{11} N/m^2)	0.596
Density ρ_e (10^3 kg/m^3)	7.47
Speed $c_e = \sqrt{B/\rho_e}$ (m/s)	2824.64

based on the maximum value within the defined domain of each image.

A. Parameter description

According to the expression of ARF, which has been obtained before, it can be learned that ARF is related to the relevant parameters. Therefore, the numerical simulation is used to explain the change in ARF under the effect of the relevant parameters intuitively. The particle material used for scattering is *Mn*. Related parameters of *Mn* are given in Table I. The environmental medium used in the simulation is water.

As shown in Fig. 1, the simulation circumstances are set. In the simulation, k is the wave number of the different order X wave, which is between 0 m^{-1} and 800 m^{-1}. z is the distance between the

transducer and particle, ranging from 0.35 m to 5.35 m. R is the radius of the particle, which is changed from 0.03 m to 0.05 m. The axicon angle of the X wave ξ ranges from 2° to 52°.

B. Spectrum of ARF exerted by the X wave

In this numerical simulation, the fixed parameters are set as follows: $z = 0.35$ m, $R = 0.035$ m, and $\xi = 2°$. k is the wave number of the different order X wave, which is between 0 m^{-1} and 800 m^{-1}. From Fig. 2, it can be found that the peak of the ARF on the sphere for the zeroth order X wave mainly appears in the range of $k = 100$ m^{-1} – 200 m^{-1} interval, which basically corresponds to the incident wave spectrum of the X wave.[40,41] Through the results of this numerical simulation, the main spectrum interval that provides ARF can be roughly determined. Therefore, acoustic tweezers can be designed through the linear combination of different orders of the X wave (in the previous theoretical derivation, the completeness of the X wave linear combination to construct any non-diffracted beam has been proved), which provides more convenience for the subsequent manipulation of specific particles. As the order of the X wave increases, the main energy interval of ARF gradually shifts to a high frequency, which is also consistent with the change in sound pressure.[40,41] The directional shift of the peaks provides the possibility to optimize the algorithm for
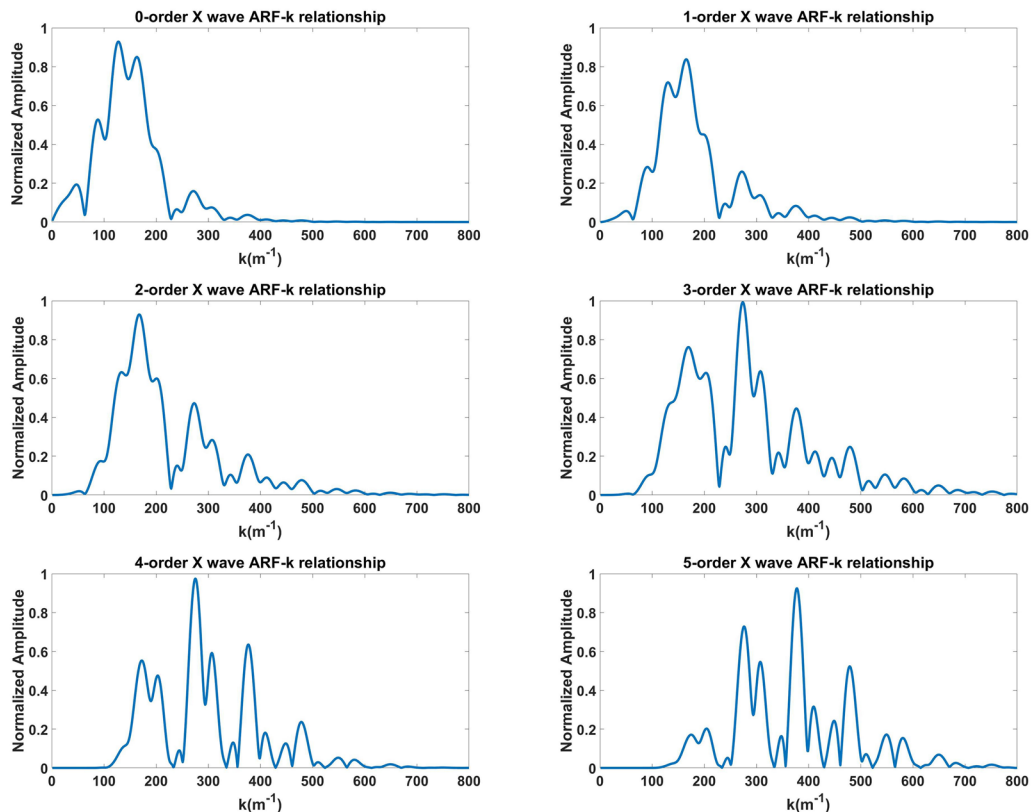
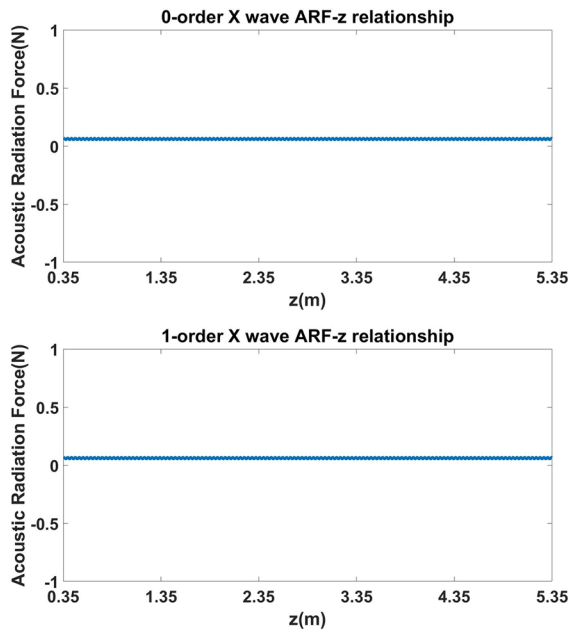FIG. 2. Spectrum of ARF generated by the different order X wave vs wave number k.

FIG. 3. ARF-z relationship. The ordinate is the ARF.

the construction of the far-field sound field. A variety of non-diffracted waves can be obtained using different combinations of X waves.

C. ARF-z relationship

In this numerical simulation, the fixed parameters are set as follows: $R = 0.035$ m and $\xi = 2°$. k is the wave number of the different order X wave, which is between 0 m^{-1} and 800 m^{-1}. z is the distance between the transducer and particle, ranging from 0.35 m to 5.35 m. Figure 3 is obtained through the calculation method of spectrum superposition. It is clear that the ARF of the zeroth and first X wave does not decay with increasing z, which also verifies the non-diffraction characteristic of the X wave. This non-diffraction property is decisive for accurate far-field construction. This has special significance for the design of acoustic tweezers. In the traditional acoustic tweezers design, limited by the diffraction effect of the beam, the acoustic control distance is constructed in a relatively small range. If the non-diffracted wave as the basic plan is taken in this paper, the range of acoustic manipulation can be greatly expanded. At the same time, this scheme jumps out of the traditional idea of constructing a fixed-position potential well and provides the possibility for stably applying thrust or traction to the particles in a larger space.
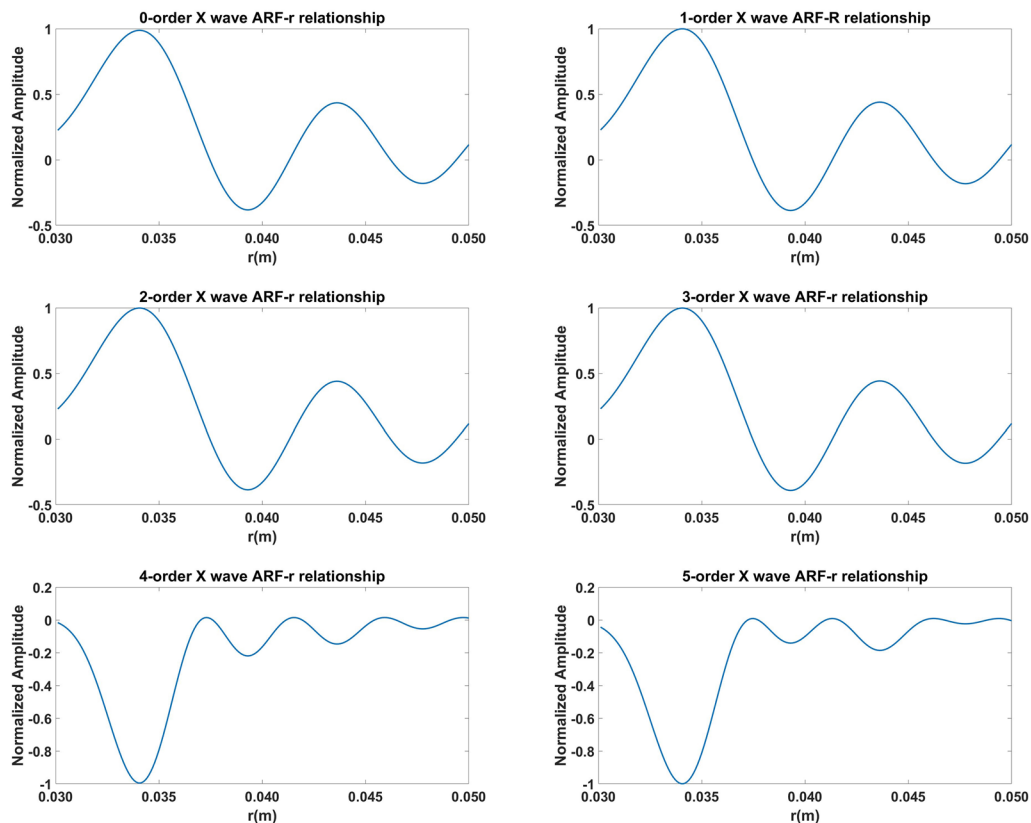

FIG. 4. ARF-R relationship. *R* represents the radius of the particle. The ordinate is the normalized ARF.
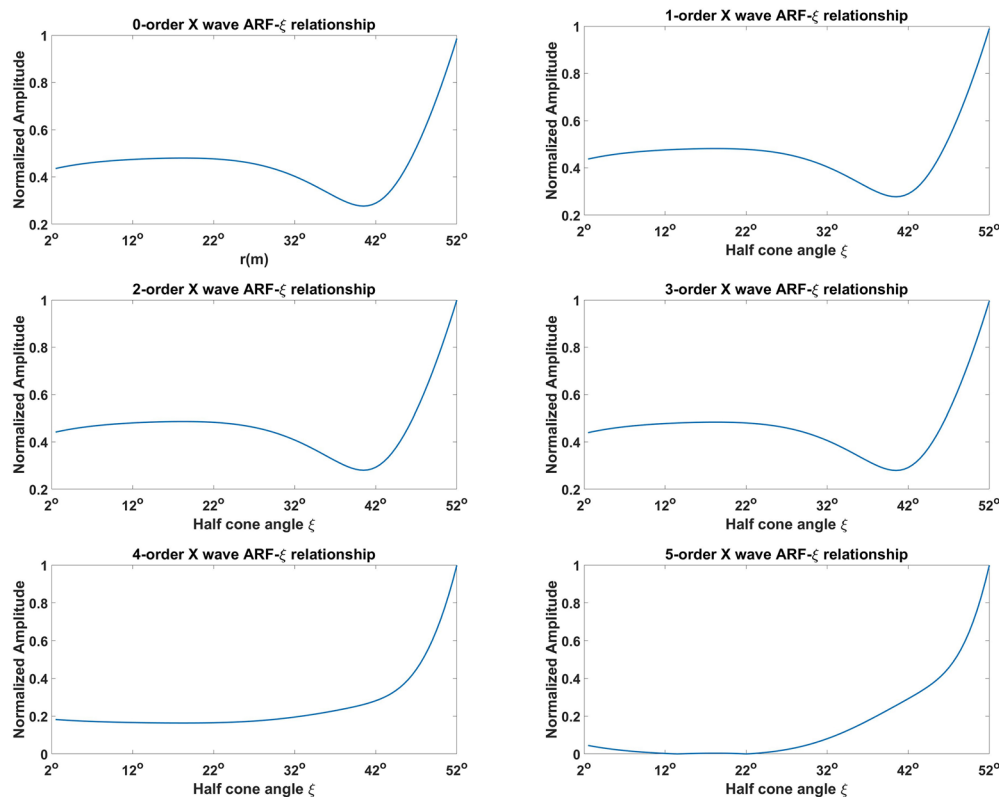
FIG. 5. ARF-ξ relationship. ξ represents the half cone angle of the X wave. The ordinate is the normalized ARF.

D. ARF-R relationship

In this numerical simulation, the fixed parameters are set as follows: $z = 0.35$ m and $\xi = 2°$. k is the wave number of the different order X wave, which is between 0 m^{-1} and 800 m^{-1}. R is the radius of the particle, which is changed from 0.03 m to 0.05 m. Figure 4 shows that within a certain range, the acoustic radiation force curve produced by the X wave on spherical particles has a wide area of negative value, which means that the effect is expressed as a pulling force. In other words, this makes it possible to construct acoustic tweezers in the far field through the X wave. In the results of this numerical simulation, it could be found that the ARF received by the particle is more sensitive to the parameter of the particle radius. It is especially worth noting that the ARF exerted by the X wave on the particles has an obvious negative range. From this targeted particle, manipulation can be carried out, such as applying a pulling force to some particles while pushing other particles to achieve particle separation. Similarly, the dynamic acceleration of the particles with the radius change in the ideal situation can be calculated, and the part of the monotonic interval can be used to achieve particle separation, such as designing a flat throw motion.

E. ARF-ξ relationship

In this numerical simulation, the fixed parameters are set as follows: $z = 0.35$ m and $R = 0.035$ m. k is the wave number of the

different order X wave, which is between 0 m^{-1} and 800 m^{-1}. The axicon angle of the X wave ξ ranges from 2° to 52°. In Fig. 5, it could be noticed that the ARFs change as the ξ increases. The changing trend of low order beams of different orders affected by the axicon angle is basically the same. Through the results of this numerical simulation, it can be seen that the angle parameter has a great influence on the design of acoustic tweezers. The amplitude of the ARF can be adjusted by the angle parameter, which is of great significance for improving the freedom of structural design of acoustic tweezers. Hence, with its monotonicity, it can be more easy to design the combination of incident X waves required for the construction of the far-field acoustic tweezers.

V. DISCUSSIONS AND CONCLUSIONS

An analytical expression of the ARF on a spherical particle illuminated by an arbitrary order X wave is deduced. The completeness and algorithmic superiority of the non-diffraction wave combination to construct the far-field sound field using the X wave as the fundamental wave are shown. The change rule of the sound radiation force generated by the X wave with various parameters is obtained and explained. Acoustic tweezers are instruments used to manipulate particles through ARF. Since the non-diffraction wave has the special property of long-distance non-diffusion, the ARF of non-diffraction wave can be used to realize the construction of far-field

acoustic tweezers. In Sec. II, the X wave as an excellent fundamental wave of non-diffracted waves is analyzed. The specific calculation proves the simplicity and completeness of the calculation using the X wave scheme for the construction of far-field acoustic tweezers using the X wave scheme. In Sec. III, the analytical expression of the ARF generated by the X wave is deduced, which lays a theoretical foundation for the design of far-field acoustic tweezers. In Sec. IV, the numerical calculations are performed using the theoretical expressions obtained, and the results of numerical calculations verify our assumptions. In Fig. 3 (ARF generated by the X wave vs the distance between the particle and the sound source), it is clearly seen that in a very large range (0.35 m–5.35 m), the X wave can provide a stable ARF. In particular, in Fig. 4 (ARF generated by the X wave vs particle radius), it is clearly seen that for particles of different radii, the X wave scheme produces a negative ARF range. This is of special significance for the construction of acoustic tweezers, which makes it possible to achieve particle pull through a single acoustic beam. For particles with a specific radius, the specific acoustic tweezers can be designed through the linear combination of X waves of different orders to capture and manipulate the particles. Moreover, the expected application scenario such as acoustic tweezers by the combination of negative acoustic radiation is explained. In addition, the invariance of the far-field ARFs of the spherical particle generated by X waves is verified, which provides the theoretical basis for far-field control of particles and the construction of the far-field acoustic manipulation environment.

ACKNOWLEDGMENTS

DATA AVAILABILITY

The data that support the findings of this study are available from the corresponding author upon reasonable request.

REFERENCES

[1] A. Ashkin, "Forces of a single-beam gradient laser trap on a dielectric sphere in the ray optics regime," Biophys. J. **61**, 569–582 (1992).

[2] J. Wu, "Acoustical tweezers," J. Acoust. Soc. Am. **89**, 2140–2143 (1991).

[3] P. Agrawal, P. S. Gandhi, and A. Neild, "Particle manipulation affected by streaming flows in vertically actuated open rectangular chambers," Phys. Fluids **28**, 032001 (2016).

[4] F. E. Chrit, S. Bowie, and A. Alexeev, "Inertial migration of spherical particles in channel flow of power law fluids," Phys. Fluids **32**, 083103 (2020).

[5] S. Li, A.-M. Zhang, S. Wang, and R. Han, "Transient interaction between a particle and an attached bubble with an application to cavitation in silt-laden flow," Phys. Fluids **30**, 082111 (2018).

[6] A. A. Mofakham and G. Ahmadi, "Particles dispersion and deposition in inhomogeneous turbulent flows using continuous random walk models," Phys. Fluids **31**, 083301 (2019).

[7] D.-Y. Zhong, G.-Q. Wang, M.-X. Zhang, and T.-J. Li, "Kinetic equation for particle transport in turbulent flows," Phys. Fluids **32**, 073301 (2020).

[8] Z. Zhou, S. Wang, X. Yang, and G. Jin, "A structural subgrid-scale model for the collision-related statistics of inertial particles in large-eddy simulations of isotropic turbulent flows," Phys. Fluids **32**, 095103 (2020).

[9] T. R. Society, R. Society, and P. Sciences, *On the Acoustic Radiation Pressure on Spheres* (Proceedings Mathematical Physical & Engineering Sciences, 1934).

[10] P. J. Westervelt, "Acoustic radiation pressure," J. Acoust. Soc. Am. **29**, 26–29 (1957).

[11] W. L. Nyborg, "Radiation pressure on a small rigid sphere," J. Acoust. Soc. Am. **42**, 947 (1967).

[12] J. Wu and G. Du, "Acoustic radiation force on a small compressible sphere in a focused beam," J. Acoust. Soc. Am. **87**, 997–1003 (1990).

[13] K. Yosioka and Y. Kawasima, "Acoustic radiation pressure on a compressible sphere," Acta Acust. Acust. **5**, 167 (1955).

[14] T. Hasegawa, M. Ochi, and K. Matsuzawa, "Acoustic radiation force on a solid elastic sphere in a spherical wave field," J. Acoust. Soc. Am. **69**, 937–942 (1981).

[15] T. Hasegawa and K. Yosioka, "Acoustic radiation force on fused silica spheres, and intensity determination," J. Acoust. Soc. Am. **58**, 581–585 (1975).

[16] X. Zhang and G. Zhang, "Acoustic radiation force of a Gaussian beam incident on spherical particles in water," Ultrasound Med. Biol. **38**, 2007–2017 (2012).

[17] M. Azarpeyvand, "Acoustic radiation force of a Bessel beam on a porous sphere," J. Acoust. Soc. Am. **131**, 4337–4348 (2012).

[18] M. Azarpeyvand, "Prediction of negative radiation forces due to a Bessel beam," J. Acoust. Soc. Am. **136**, 547–555 (2014).

[19] D. Baresch, J.-L. Thomas, and R. Marchiano, "Three-dimensional acoustic radiation force on an arbitrarily located elastic sphere," J. Acoust. Soc. Am. **133**, 25–36 (2013).

[20] D. Baresch, J.-L. Thomas, and R. Marchiano, "Observation of a single-beam gradient force acoustical trap for elastic particles: Acoustical tweezers," Phys. Rev. Lett. **116**, 024301 (2016).

[21] X.-D. Fan and L. Zhang, "Trapping force of acoustical Bessel beams on a sphere and stable tractor beams," Phys. Rev. Appl. **11**, 014055 (2019).

[22] Z. Gong, P. L. Marston, W. Li, and Y. Chai, "Multipole expansion of acoustical Bessel beams with arbitrary order and location," J. Acoust. Soc. Am. **141**, El574–El578 (2017).

[23] W. Li and M. Wang, "Scattering of an arbitrary order acoustical Bessel beam by a rigid off-axis spheroid," J. Acoust. Soc. Am. **143**, 3676–3687 (2018).

[24] P. L. Marston, "Axial radiation force of a Bessel beam on a sphere and direction reversal of the force," J. Acoust. Soc. Am. **120**, 3518–3524 (2006).

[25] P. L. Marston, "Negative axial radiation forces on solid spheres and shells in a Bessel beam," J. Acoust. Soc. Am. **122**, 3162–3165 (2007).

[26] P. L. Marston, "Radiation force of a helicoidal Bessel beam on a sphere," J. Acoust. Soc. Am. **125**, 3539–3547 (2009).

[27] Y. Qiao, J. Shi, X. Zhang, and G. Zhang, "Acoustic radiation force on a rigid cylinder in an off-axis Gaussian beam near an impedance boundary," Wave Motion **83**, 111–120 (2018).

[28] Y. Qiao, X. Zhang, and G. Zhang, "Acoustic radiation force on a fluid cylindrical particle immersed in water near an impedance boundary," J. Acoust. Soc. Am. **141**, 4633–4641 (2017).

[29] O. A. Sapozhnikov and M. R. Bailey, "Radiation force of an arbitrary acoustic beam on an elastic sphere in a fluid," J. Acoust. Soc. Am. **133**, 661–676 (2013).

[30] H. B. Wang, S. Gao, Y. P. Qiao, J. H. Liu, and X. Z. Liu, "Theoretical study of acoustic radiation force and torque on a pair of polymer cylindrical particles in two airy beams fields," Phys. Fluids **31**, 047103 (2019).

[31] R. Wu, K. Cheng, X. Liu, J. Liu, X. Gong, and Y. Li, "Study of axial acoustic radiation force on a sphere in a Gaussian quasi-standing field," Wave Motion **62**, 63–74 (2016).

[32] R. Wu, K. Cheng, X. Liu, J. Liu, Y. Mao, and X. Gong, "Acoustic radiation force on a double-layer microsphere by a Gaussian focused beam," J. Appl. Phys. **116**, 144903 (2014).

[33] R. Wu, X. Liu, and X. Gong, "Axial acoustic radiation force on a sphere in Gaussian field," Recent Dev. Nonlinear Acoust. **1685**, 040010 (2015).

[34] L. Zhang, "A general theory of arbitrary Bessel beam scattering and interactions with a sphere," J. Acoust. Soc. Am. **143**, 2796–2800 (2018).

[35] L. Zhang and P. L. Marston, "Geometrical interpretation of negative radiation forces of acoustical Bessel beams on spheres," Phys. Rev. E **84**, 035601 (2011).

[36] L. Zhang and P. L. Marston, "Axial radiation force exerted by general non-diffracting beams," J. Acoust. Soc. Am. **131**, El329–El335 (2012).

[37] S. Z. Hoque and A. K. Sen, "Interparticle acoustic radiation force between a pair of spherical particles in a liquid exposed to a standing bulk acoustic wave," Phys. Fluids **32**, 072004 (2020).

[38] F. G. Mitri, "Radiation forces and torque on a rigid elliptical cylinder in acoustical plane progressive and (quasi)standing waves with arbitrary incidence," Phys. Fluids **28**, 077104 (2016).

[39] P. L. Marston, "Comment on 'Radiation forces and torque on a rigid elliptical cylinder in acoustical plane progressive and (quasi)standing waves with arbitrary incidence' [Phys. Fluids 28, 077104 (2016)]," Phys. Fluids **29**, 029101 (2017).

[40] M. F. Moawad, A. M. Shaarawi, and I. M. Besieris, "Characterization of a non-rigid sphere using the backscattered fields of acoustic x waves," J. Acoust. Soc. Am. **115**, 2937–2946 (2004).

[41] J.-Y. Lu and J. F. Greenleaf, "Nondiffracting X waves-exact solutions to free-space scalar wave equation and their finite aperture realizations," IEEE Trans. Ultrason. Ferroelectr. Freq. Control **39**, 19–31 (1992).